Tropical Cyclogenesis within an Equatorial Rossby Wave Packet

JOHN MOLINARI, KELLY LOMBARDO,* AND DAVID VOLLARO

Department of Earth and Atmospheric Sciences, University at Albany, State University of New York, Albany, New York

ABSTRACT

A packet of equatorial Rossby (ER) waves that lasted 2.5 months is identified in the lower troposphere of the northwest Pacific. Waves within the packet had a period of 22 days, a wavelength of 3600 km, a westward phase speed of 1.9 m s^{-1}, and a near-zero group speed. The wave properties followed the ER wave dispersion relation with an equivalent depth near 25 m. The packet was associated with the development of at least 8 of the 13 tropical cyclones that formed during the period. A composite was constructed around the genesis locations. Tropical cyclones formed east of the center of the composite ER wave low in a region of strong convection and a separate 850-hPa vorticity maximum.

The background flow during the life of the packet was characterized by 850-hPa zonal wind convergence and easterly vertical wind shear. Wave amplitude peaked at the west end of the convergent region, suggesting that wave accumulation played a significant role in the growth of the packet. The presence of easterly vertical wind shear provided an environment that trapped energy in the lower troposphere. Each of these processes increases wave amplitude and thus the likelihood of tropical cyclone formation within the waves.

The initial low pressure region within the wave packet met Lander's definition of a monsoon gyre. It developed to the west of persistent localized convection that followed the penetration of an upper-tropospheric trough into the subtropics. It is argued that the monsoon gyre represented the initial ER wave low within the packet.

1. Introduction

A great deal of research has been carried out describing the linear shallow-water solutions for waves on an equatorial beta plane (hereafter simply "equatorial waves") following the pioneering work of Matsuno (1966) and Lindzen (1967). Evidence for such waves in nature has been described by Yanai and Maruyama (1966), Wallace and Kousky (1968), and many researchers since. More recently, Takayabu (1994), Wheeler and Kiladis (1999), and Roundy and Frank (2004) described the climatology of such waves in wavenumber–frequency space using measures of outgoing infrared radiation (OLR) or precipitable water fields.

Because the waves were described using cloud and moisture fields, they represented convectively coupled, lower-tropospheric waves. The waves contained small equivalent depths of 12–50 m, indicative of tropospheric vertical wavelengths of 7–13 km (Wheeler et al. 2000). These studies showed the dominance of equatorial wave modes between 15°N and 15°S. Other than the Madden–Julian oscillation (MJO), and in northern summer off-equatorial easterly waves, no other part of the wavenumber–frequency space contained significant return above a smoothed background. Because equatorial wave modes play a major role in the variation of OLR between 15°N and 15°S, they might substantially influence tropical cyclogenesis in that region as well.

Limited evidence for a role of equatorial waves in tropical cyclogenesis has been given in the literature. (In this paper "wave" will represent a generic term for a disturbance whose characteristics suggest a wavelike origin; thus the term could include disturbances that have developed closed vorticity contours as they intensified and interacted with convection). Nitta and Takayabu (1985) tracked 5–10-day disturbances that were associated with western Pacific tropical cyclogen-

---

* Current affiliation: Institute for Terrestrial and Planetary Atmospheres, Stony Brook University, Stony Brook, New York.

Corresponding author address: John Molinari, Department of Earth and Atmospheric Sciences, University at Albany, State University of New York, ES351, Albany, NY 12222.
E-mail: molinari@atmos.albany.edu

esis back to a point near the equator and 170°E. The origin point suggests the disturbances were some form of equatorial wave mode. Chang et al. (1996) found northwestward-propagating waves of 8–9-day period that also originated near the equator. During periods that such disturbances had large variance, tropical cyclones were much more likely to form. Takayabu and Nitta (1993) identified mixed Rossby–gravity (MRG) waves in the central Pacific that turned away from the equator near 150°E and appeared to transition to "TD-type" disturbances (i.e., Rossby-type waves, also known as easterly waves). They showed one example of a tropical cyclone forming within such a TD-type disturbance. Dickinson and Molinari (2002) described a MRG wave packet that lasted one month. Disturbances within the packet propagated westward along the equator, then northwestward away from the equator. Three tropical cyclones formed in association with three consecutive lows within the packet in a two-week period. The tropical cyclones did not form in the center of the lows, but to their east, where the linear MRG wave solution gives maximum convergence. Although the formation occurred only after the MRG vorticity centers had turned off the equator, there seemed little doubt that the tropical cyclones were forming in waves of equatorial origin.

All of the above tropical cyclogenesis studies involved waves with periods in the range 5–10 days. In contrast, Yamazaki and Murakami (1989) examined 20–40-day westward-propagating waves in the meridional wind averaged 6°–16°N. They found that western Pacific tropical cyclogenesis was most common when the amplitude of these waves was large. The authors identified the waves as an intraseasonal oscillation, but the characteristics are consistent with $n = 1$ equatorial Rossby (ER) waves. Hartmann et al. (1992) described waves of 20–25-day period in the western Pacific that carried substantial variance in late boreal summer and fall. The composite unfiltered flow during the time these oscillations were large in amplitude showed low pressure first appearing near the date line on the equator, then propagating westward and expanding poleward in the Northern, but not Southern, Hemisphere. A smaller-scale low deepened near 10°N, then moved westward and northward to 20°N. The cycle repeated with opposite sign, starting with high pressure appearing near the date line. Once again the characteristics suggest ER wave involvement, although none was specifically suggested. Hartmann et al. (1992) noted that tropical cyclogenesis was, by far, most frequent during the parts of the cycle when the strong low was present in the Northern Hemisphere.

Numaguti (1995) examined the formation of six tropical cyclones in the western Pacific during the Tropical Ocean Global Atmosphere Coupled Ocean–Atmosphere Response Experiment (TOGA COARE). He argued, based on somewhat indirect evidence, that each genesis event occurred either in association with a MRG wave or an ER wave. More recently, Bessafi and Wheeler (2006) found that tropical cyclogenesis in the south Indian Ocean was modulated strongly by ER waves, weakly by Kelvin waves, and not at all by MRG waves. Frank and Roundy (2006) found similar results in the south Indian Ocean, but in other regions found that tropical cyclones developed in the presence of enhanced activity of MRG and ER waves, but not Kelvin waves. Bessafi and Wheeler (2006) showed that genesis occurred both east and west of ER wave lows, whereas Frank and Roundy's (2006) composite showed development occurring several hundred kilometers southeast of the ER wave low centers.

A number of authors have noted the importance of background flow variations in producing synoptic-scale disturbance growth, and thus increasing the likelihood of tropical cyclogenesis. Background flow variations can be produced by the MJO and the climatological trade winds and monsoon trough. This topic will be addressed further when the background flow for the storms in this study is examined.

The above studies provide evidence for tropical cyclone formation within equatorial wave modes, but few specific case studies have been carried out that describe the role of the waves and the background flow in the cyclogenesis. The current work will identify repeated tropical cyclogenesis within a packet of ER waves in the western North Pacific.

Choice of a case study

This work did not begin as a study of equatorial wave modes. Instead, as in the study of Dickinson and Molinari (2002), the equatorial waves emerged from the investigation of a seemingly unrelated phenomenon. Of interest was the work by Lander (1994), who described a "monsoon gyre" (a subtropical low of 2500 km diameter) during August and September of 1991 that spawned six tropical cyclones in 20 days. Holland (1995) studied the same gyre. He argued that convergence associated with the remains of a frontal zone from middle latitudes played a significant role in the creation of the gyre and provided a favorable environment for wave growth and tropical cyclone development.

The initial aim of the current study was to further understand the formation of the 1991 gyre and its role in tropical cyclogenesis. As the study proceeded, however, it became apparent that the gyre was part of a

longer-lasting ER wave packet. Because the packet appeared to represent the fundamental dynamical component of the flow, the emphasis of the study changed. The results to follow will describe the evolution of the packet, the role of environmental factors in its development and maintenance, and the repeated tropical cyclogenesis that occurred within it.

2. Data and methods

This study makes use of two sources of data: analyses from the European Centre for Medium-Range Weather Forecasts (ECMWF) on a 1.125° latitude–longitude grid and outgoing longwave radiation (OLR) on a 2.5° grid [Liebmann and Smith (1996) and upgraded by G. Kiladis (2003, personal communication)]. The OLR data were bilinearly interpolated to 1.125° to allow overlay with winds and vorticity. A number of previous studies have shown that global gridded analyses from operational centers contain detailed information on equatorial wave modes that is consistent with independently measured fields like OLR (e.g., Wheeler et al. 2000; Dickinson and Molinari 2002). Because the equatorial wave modes of interest in this study are synoptic scale, the enormous data streams that enter the operational analysis cycle are sufficient to produce a meaningful description of their evolution.

Evidence will be presented that the waves in this study are ER waves. Unfiltered fields did not always clearly display the waves. Instead, a bandpass filter with 15-day and 40-day half-power points (Lanczos 1956) was used. The half-power points were similar to those used previously by Yamazaki and Murakami (1989) and Hartmann et al. (1992).

Use of a 15–30-day bandpass filter produced virtually identical time series, indicating that little power existed in the 30–40-day range. The coherence of the ER wave packet was reduced, however, with a 10–40-day filter. This might reflect the influence of other wave types, tropical cyclones, or background noise. As a result, all subsequent figures make use of the 15–40-day filter to describe the wave packet.

Wheeler and Kiladis (1999) used a more extensive process in order to isolate individual equatorial wave modes. It required filtering in both time and space and formal separation by equatorial symmetry and by the direction of propagation. The simple time filtering used in this paper allows other disturbances to enter beyond the $n = 1$ ER waves of interest. No additional filtering was done for several reasons. First, removing the symmetry constraint allows study of equatorial waves that experience complex shears and hemispheric asymmetry, yet still contain many properties of the modal so-

TABLE 1. Phase speeds (m s^{-1}) of $n = 1$ equatorial Rossby waves for various wavelengths and equivalent depths. Values include the influence of a time-mean and space-mean background zonal flow $U = 0.92$ m s^{-1}. The effects of zonal flow beyond simple Doppler shifting are included following Zhang and Webster (1989) and Kiladis and Wheeler (1995).

	$H =$		
L (km)	12 m	25 m	50 m
2000	−0.71	−0.86	−0.98
3000	−1.52	−1.95	−2.35
4000	−2.05	−2.74	−3.47
5000	−2.37	−3.28	−4.30
6000	−2.59	−3.65	−4.89
7000	−2.73	−3.90	−5.32
8000	−2.82	−4.08	−5.64
9000	−2.89	−4.21	−5.87
10 000	−2.95	−4.31	−6.05

lution (Straub and Kiladis 2002; Roundy and Frank 2004). The ER waves in this study will be shown to be asymmetric with respect to the equator. Second, the ER waves will be shown to have amplified in a region of horizontal convergence of the background flow, and their horizontal scale changed with time. In principle such waves would remain within the ER space–time filter shown by Wheeler and Kiladis (1999). Shorter ER wavelengths, however, contain phase speeds close in magnitude to background zonal wind speeds. For this reason the waves might deviate from the ER spectral region defined by Wheeler and Kiladis (1999), who assumed zero zonal wind. Third, little evidence existed for significant 15–40-day eastward-propagating disturbances in this study, minimizing the need to separate out eastward and westward propagation. Finally, the simple time filtering carried out here produced a remarkably well-defined wave packet. It was concluded that no further filtering was necessary.

To give support for the diagnosis of ER waves, the observed phase and group velocity will be compared with those from the linear shallow-water solution for the observed wavelengths and background zonal flow. These calculations will follow the approach of Zhang and Webster (1989), using the dimensional forms of the equations given by Kiladis and Wheeler [1995, their appendix equations (A1) and (A2)]. The Zhang and Webster equations allow for the effects of a nonzero zonal flow beyond simply Doppler shifting. The zonal flow U in these equations will be defined as the 850-hPa temporal and spatial mean over the wave packet (14 August–30 October 1991, from 5°–20°N to 125°–155°E), which gives $U = 0.92$ m s^{-1}. The mean of a 40-plus-day, low-pass filtered zonal wind differed by less than 0.1 m s^{-1}. Tables 1 and 2 give the calculated

TABLE 2. As in Table 1 but for the $n = 1$ ER wave group speed.

L (km)	$H =$		
	12 m	25 m	50 m
2000	1.21	1.55	1.87
3000	0.44	0.89	1.45
4000	−0.41	−0.13	0.39
5000	−1.08	−1.08	−0.80
6000	−1.56	−1.84	−1.88
7000	−1.91	−2.42	−2.77
8000	−2.17	−2.86	−3.48
9000	−2.36	−3.20	−4.04
10 000	−2.50	−3.45	−4.49

phase and group speeds, respectively, for a range of wavelengths and for the three equivalent depths shown by Wheeler and Kiladis (1999).

3. Equatorial Rossby wave packet

a. Structure of the packet

Figure 1a shows a longitude–time series of unfiltered meridional wind at 850 hPa over the western Pacific from mid July until the end of October 1991, averaged from 5° to 20°N. Westward-moving disturbances predominated. A possible wave packet is suggested by Fig. 1a, but it is obscured by the mean flow and by other phenomena, including tropical cyclones. Figure 1b shows the same field after bandpass filtering with half-power points at 15 and 40 days. A striking wave packet emerges. It initiated before the middle of August and lasted until late October. Its amplitude was about 4–5 m s^{-1} in the meridional wind.

Wavelength, period, and/or phase speed of waves in the packet can be estimated in principle from the Hovmöller diagram. In practice, phase speed was most subject to truncation error on the 1.125° grid and was, instead, determined from the other two variables. Wavelength was estimated by doubling the distance between the maxima and minima in the v component at each time. Period was estimated by the time between consecutive maxima or consecutive minima. The mean wavelength and period were 3600 km and 22 day, with estimates varying by ±10% over the life of the packet. This gives a mean phase speed of −1.9 m s^{-1}. By inspection, the group speed stayed close to zero. The "G" in Fig. 1b represents an estimate of the first appearance at 15°N in the unfiltered wind field of the monsoon gyre described by Lander (1994). This feature will be addressed further in section 3d.
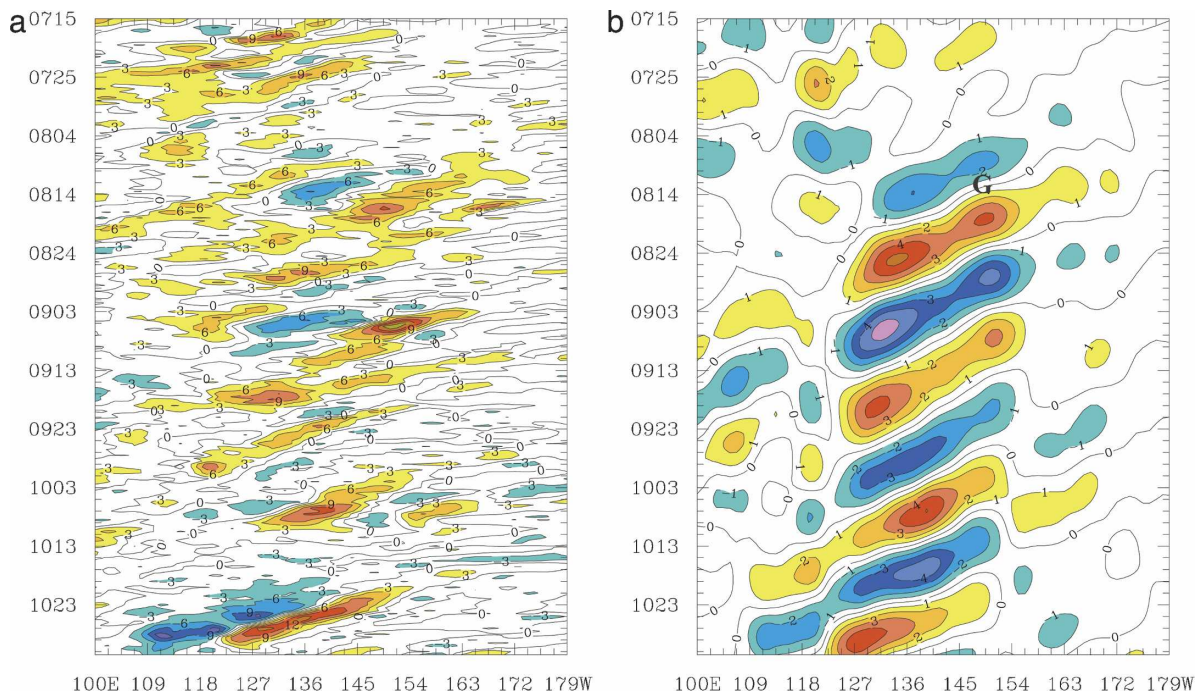

FIG. 1. Longitude–time series of 850-hPa meridional wind, averaged 5°N–20°N, for the period 15 Jul–30 Oct 1991. (a) Unfiltered and (b) bandpass-filtered with half-power points at 15 and 40 days. Contour increment is (a) 3 m s^{-1} and (b) 1 m s^{-1}. Shading in warm and cool colors represents, respectively, southerly and northerly wind components exceeding (a) 3 m s^{-1} and (b) 1 m s^{-1}. The letter "G" indicates the initial appearance at 15°N of the monsoon gyre described by Lander (1994) and discussed in section 3d of this paper.

Because the disturbances in question have the time scale of $n = 1$ ER waves, propagate westward, have zero group speed, and are characterized by their off-equatorial v component, Fig. 1b appears to represent an ER wave packet. Tables 1 and 2 show that for 3000–4000-km wavelengths and $U = 0.92$ m s^{-1}, the linear shallow water phase and group speed fall close to their observed values of -1.9 and 0.0 m s^{-1}, respectively, for an equivalent depth near 25 m. This equivalent depth is consistent with the results of Wheeler and Kiladis (1999). In contrast, the phase and group speed for non-divergent barotropic Rossby waves of 4000-km wavelength and the same zonal wind are -8.4 and 10.2 m s^{-1}, respectively, far from those observed.

Kiladis and Wheeler (1995) noted that the linearized primitive equations are not strictly separable into shallow water and vertical components in the presence of vertical wind shear. It will be shown (Fig. 11) that easterly vertical shear is present in the region of interest in this paper. As a result, the close match of both phase and group speed to a shallow water solution with 25-m equivalent depth for the observed 3600-km wavelength in Tables 1 and 2 might be somewhat fortuitous. Even so, there seems little doubt that the observed wave packet represents ER waves rather than any possible alternative.

Equatorial Rossby waves can be represented by the equatorial zonal wind as well as off-equatorial meridional wind (e.g., see Fig. 10 from Wheeler et al. 2000). Figure 2 shows a longitude–time diagram for the same period as Fig. 1, but for the bandpass-filtered zonal wind averaged from 0° to 5°N. Paradoxically, the properties of the resulting wave packet differed from those shown in Fig. 1b. The waves in Fig. 2 have a wavelength of about 9500 km (near-zonal wavenumber 4) and move westward at approximately 5 m s^{-1}, but keep the same period (22 day) shown by the v component. These characteristics are virtually identical to those of composite equatorial Rossby waves in the western Pacific described by Wheeler et al. (2000). It will be shown later that the differing wavelengths at the equator and 5°–20°N can be accounted for by the differences in background flow in the two regions. The key aspect of Fig. 2 for this study is that relatively small amplitude long waves appear to come from the east throughout the period of the wave packet.

Figure 3 shows a series of x–y plots of wind vectors and OLR within the wave packet, each bandpass filtered as in Fig. 1b. These weather maps are shown in 11-day increments (half the wave period) from 14 August to 30 October 1991. Figures 3a and 3b do not give a clear indication of shallow water ER structure. Rather, a large low pressure area near 15°N, 150°W
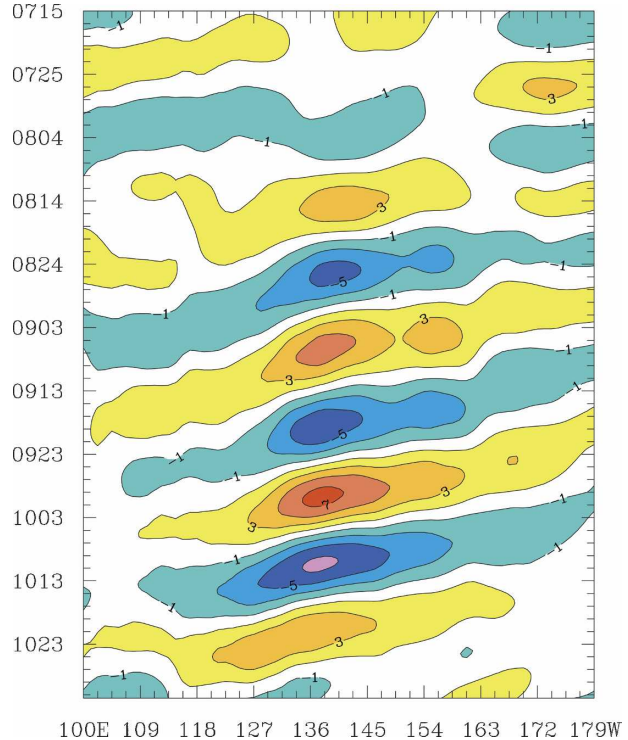

FIG. 2. As in Fig. 1b but for zonal wind averaged 0°–5°N, with contour increment of 2 m s^{-1} (no zero line). Shading in warm and cool colors represents, respectively, westerly and easterly wind components exceeding 1 m s^{-1}.

(indicated by the symbol "L1") moved westward, then northward, while shrinking in scale. Disturbance L1 corresponds to the monsoon gyre of Lander (1994). No evidence of a Southern Hemisphere reflection of the low existed, unlike the shallow water solution for ER waves. Above-average convection extended south and east of the low. After one-half period, the low was replaced by a high (H1) in a similar location.

After an additional half period (5 September; Fig. 3c), a strong low (L2) again appeared at 15°N. In contrast to the previous wave period, a second low was present in the Southern Hemisphere, also labeled L2, reflecting the expected pair of lows with ER waves. The previous high (H1) had moved westward and northward and contracted in scale like L1 before it. By 16 September (Fig. 3d), the Northern Hemisphere L2 had also moved westward, then northward. There was no longer evidence of the Southern Hemisphere L2. Two high pressure areas (H2) appeared on 16 September, closer to the equator in each hemisphere than the previous lows.

The linear shallow water solution for ER waves contains convergence one-quarter wavelength east of the low. This convergence pattern was reflected in the
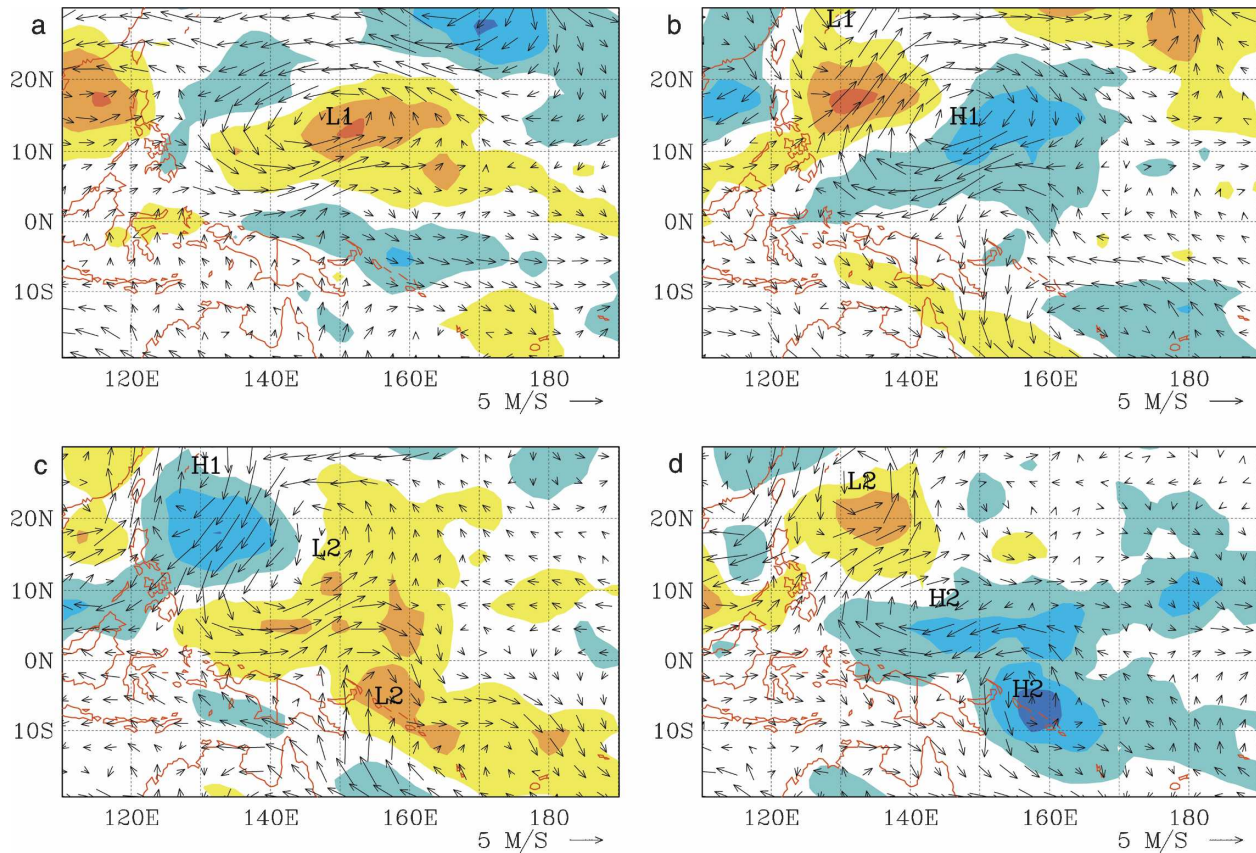
FIG. 3. Evolution of 15–40-day bandpass-filtered 850-hPa wind and OLR (shaded), shown every 11 days (i.e., increments of one-half period) during the life of the equatorial Rossby packet, valid at 0000 UTC on (a) 14 Aug, (b) 25 Aug, (c) 5 Sep, (d) 16 Sep, (e) 27 Sep, (f) 8 Oct, (g) 19 Oct, and (h) 30 Oct 1991. Warm colors indicate OLR anomalies of -10, -30, and -50 W m^{-2}. Cool colors represent OLR anomalies of 10, 30, and 50 W m^{-2}. Each L and H tracks a particular low or high, respectively.

negative OLR anomalies east, but not west, of the low in Fig. 3c. In other respects the wave structure differed from the shallow water solution. Above-average convection existed equatorward as well as east of the low centers. The twin low pressure areas did not occur at the same longitude, and were not symmetric about the equator, but shifted northward. The lows contained neither the same amplitude nor horizontal scale. It is notable, however, that the structure shown in Figs. 3c,d closely resembles the composite western Pacific ER wave shown by Wheeler et al. (2000, their Fig. 9b). These authors constrained ER waves to follow symmetry constraints and fit strictly within the linear shallow water solutions. Nevertheless, their composite ER wave also contained a Southern Hemisphere low that was smaller and farther east than that to the north and contained almost identical OLR anomaly structure. In addition, their Hovmöller diagram of the composite ER wave barely contained one full wavelength in space at any given time, much like Fig. 1b. Recently Frank and Roundy (2006) showed ER wave composites during cy-

clogenesis events in the western Pacific that also resembled Figs. 1b and 3c,d. As a result, although the observed structure deviates from the shallow water solution, the packet is almost certainly made up of equatorial Rossby waves.

Figures 3e,f continue to show a similar evolution of waves in the packet, except that L3 and H3 lie at 10°N. Figures 3g,h show the same structure but with amplitude beginning to decrease. In addition, the ER structure seemed to disappear in the final panel on 30 October, which shows a Northern Hemisphere reflection of H4, but little indication of a Southern Hemisphere signature. The packet was assumed to end at this time.

b. Evolution of the packet

Figures 3a–f showed the wave packet each half period, when the respective lows and highs achieved their largest amplitude. In this section the evolution will be examined in more detail (every three days) for one full period beginning near the maximum amplitude of the two L2 lows. Figure 4a begins just two days after the
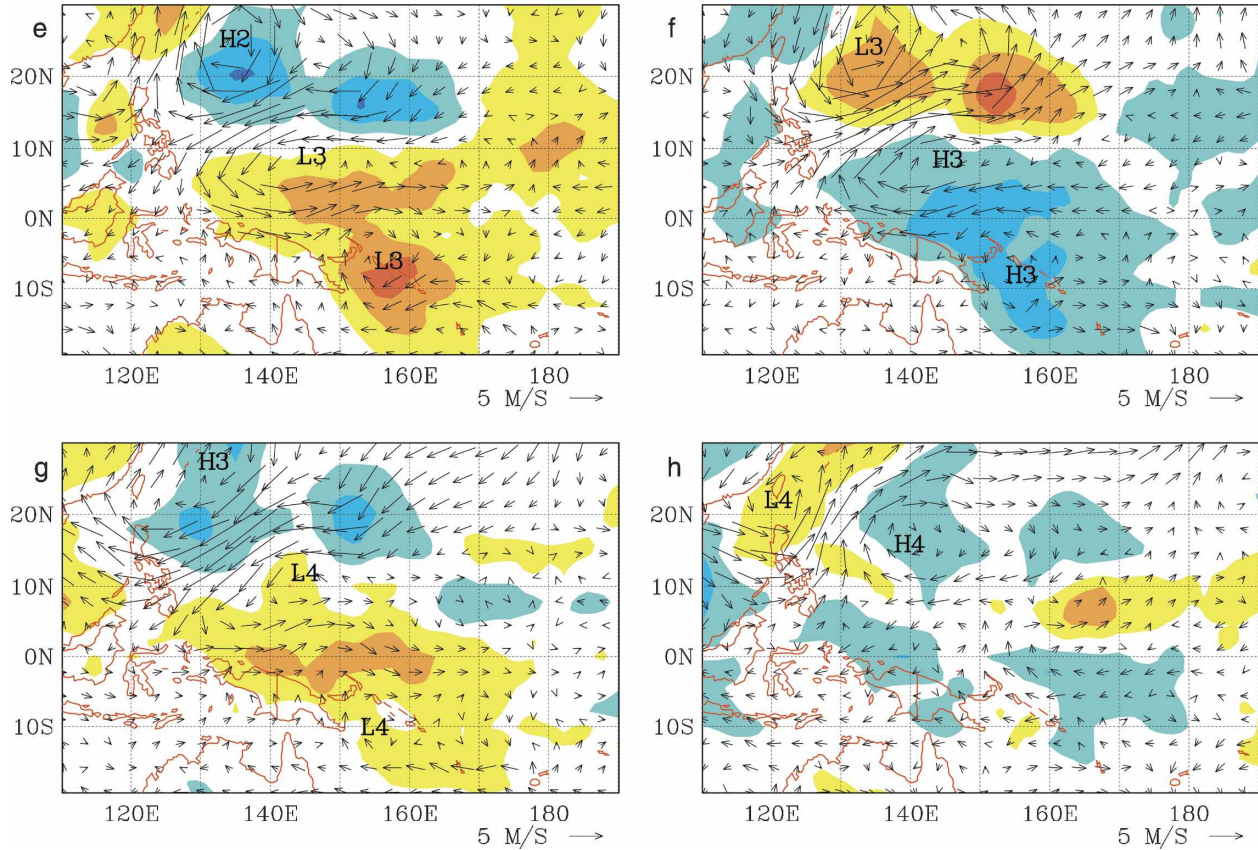
FIG. 3. (*Continued*)

time in Fig. 3c, when the ER wave structure had become established. It shows the Northern Hemisphere low near 15°N and the smaller, weaker low near 10°S. Large regions of above-average convection were present, especially equatorward and eastward of these lows. Much farther east, near the date line, positive OLR anomalies on the equator gave the first indication of the ER wave highs to come. By 10 September, three days later (Fig. 4b), the northern L2 had moved westnorthwestward. The convection well to its east and southeast began to weaken. The southern L2 moved poleward and lost much of its convective signature. The positive OLR anomalies on the equator near the date line extended westward and grew in area. The first evidence of a pair of high pressure areas was present near 5°N and 5°S at 175°E. By 13 September (Fig. 4c), the northern L2 had weakened, lost most of its convective signature, and decreased in scale as it moved westward. The southern L2 could not be found. The area of below-average convection continued to expand poleward in each hemisphere. Positive OLR anomalies at the equator covered nearly 50° longitude. This implies a wavelength close to 10 000 km, consistent with that

shown by the *u*-component time series from Fig. 2. Anticyclonic circulation was present close to the equator in each hemisphere. The boreal signature was better defined and extended over a larger longitudinal region. On 16 September (Fig. 4d), the northern low L2 moved poleward and reintensified, and a strong convective anomaly redeveloped just to its south. Well-defined anticyclones were present near 10°N and 5°S, each labeled H2. The convective minima with these highs became distinct in each hemisphere. The highs contained the same zonal and meridional asymmetries that were seen previously in the lows.

On 19 September (Fig. 4e), the northern L2 hardly moved while continuing to intensify. The northern H2 moved westward along 10°N, and the southern H2 moved westward and poleward. The positive OLR anomalies weakened in both H2 highs. The first signs of a negative OLR anomaly appeared at the equator and 170°E. By 22 September (Fig. 4f), each H2 moved westward and slightly poleward. The negative OLR anomaly extended westward along the equator and expanded poleward in each hemisphere. The last two panels show the development of a pair of L3 lows, which
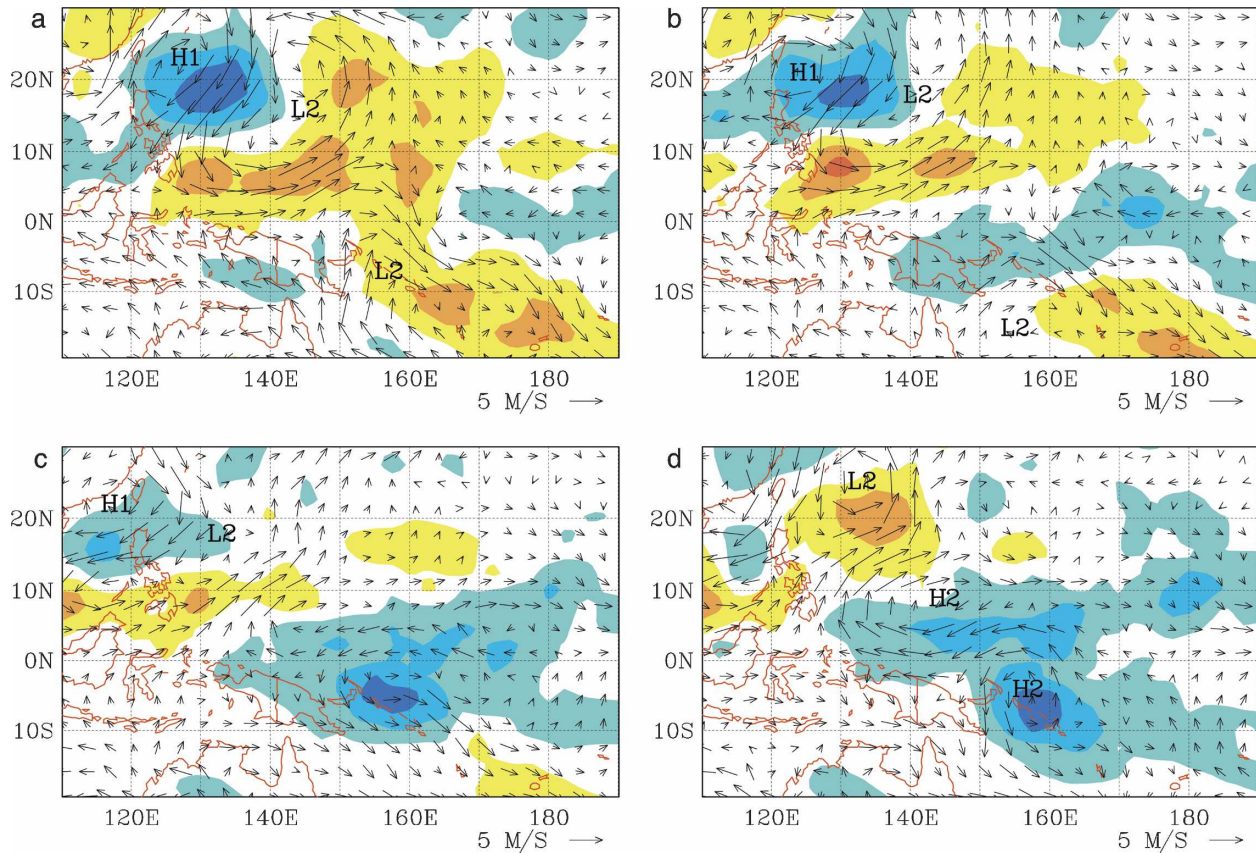
FIG. 4. As in Fig. 3 but, shown every three days in September 1991, depicting the evolution during a single ER wave period: (a) 7, (b) 10, (c) 13, (d) 16, (e) 19, (f) 22, (g) 25, and (h) 28 Sep 1991.

evolved similarly to L1 and H2 previously. As before, the equatorial OLR anomalies covered 50° of longitude.

The sequence shown in Fig. 4 resembles the composite structure of waves of almost the same period shown by Hartmann et al. (1992). They found a signature in the pressure field at the equator near the date line, consistent with the OLR signature in Fig. 4. The period of their waves, as well as the off-equatorial growth and emanation of disturbances toward middle latitudes, were almost identical to those in this study. It appears likely that Hartmann et al. (1992) were describing ER waves.

Figures 1–4 showed a long-lasting ER wave packet. Between 5° and 20°N, waves within the packet decreased in scale and increased in amplitude compared to their properties east of 150°E. Consistent with Table 1, westward phase speed slowed as the waves decreased in scale, and eventually their westward motion ceased. Paradoxically, wavelengths and phase speeds remained large, while the period remained the same, at the equator. In the Southern Hemisphere, the wave packet was much less well defined. Several questions arise: Why

was the packet so strong and long lasting? Why did it differ in structure with latitude? How did it modulate tropical cyclogenesis? In the following section, the role of background convergence and vertical wind shear will be reviewed. Their possible roles in the wave behavior will be described.

c. Large-scale environment of the packet

The most relevant work on the role of background flow on ER waves was done by Webster and Chang (1988, 1997), Chang and Webster (1990), Wang and Xie (1996), and Xie and Wang (1996). Webster and Chang (1988) examined the behavior of ER waves in the western Pacific in the presence of background zonal divergence u_x (they described u_x as stretching deformation; the two are equivalent when only the zonal component is considered). Webster and Chang (1988) described a wave accumulation process produced by $u_x < 0$ in which waves increase in amplitude and decrease in scale in the manner described by Lighthill (1978). They showed that equatorial Rossby waves can eventually turn poleward out of the equatorial waveguide as they amplify. The zonal flow used by these authors was rep-
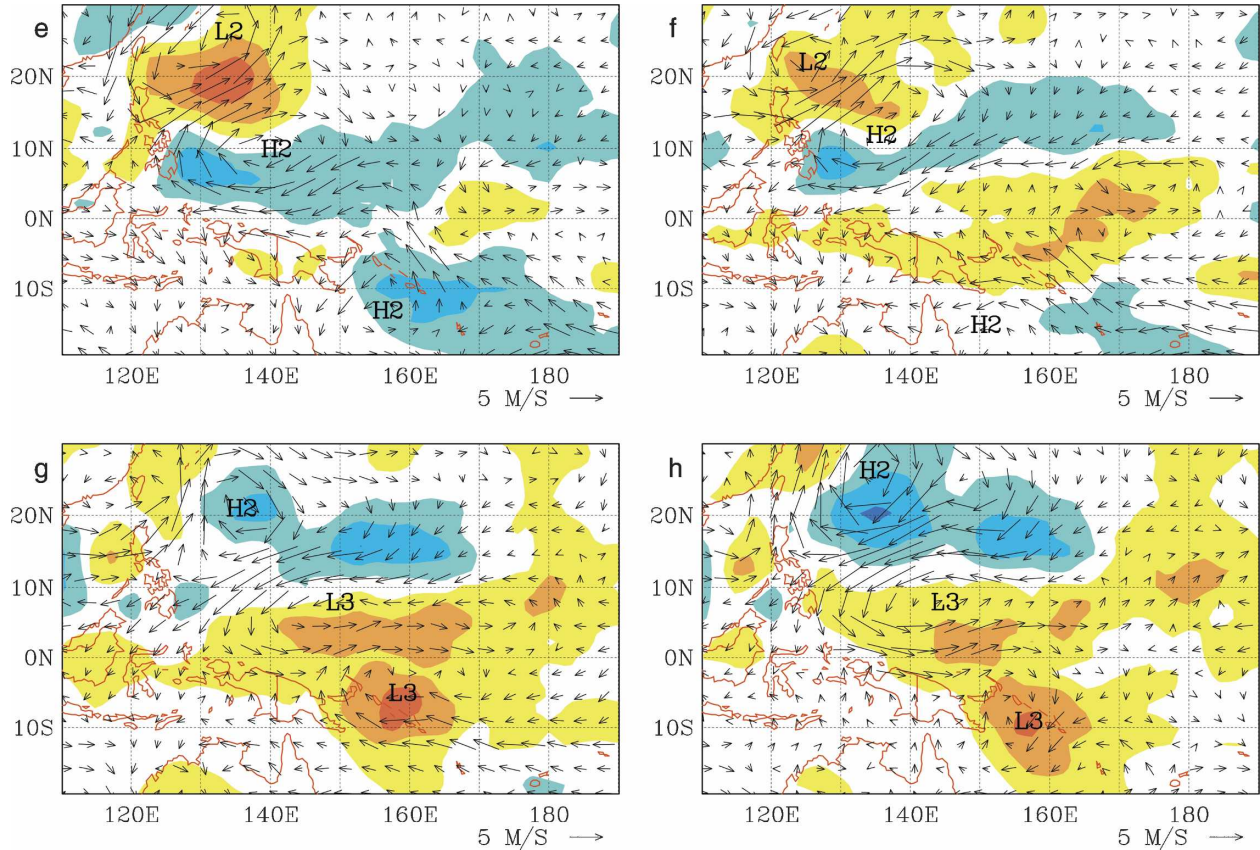
FIG. 4. (*Continued*)

resentative of the upper troposphere. In addition, they examined ER waves with 200-m equivalent depth, much larger than in this study. Nevertheless, the same concepts hold in principle wherever background convergence is present.

The term "wave accumulation" is not strictly valid in most circumstances in nature because the waves often develop closed (unwavelike) vorticity contours as they intensify. Nevertheless, the existence of wave packets whose properties resemble those described by dispersion relations suggests that the concept has some relevance. Use of this terminology is supported by the work of Sobel and Bretherton (1999). They showed that, in the western Pacific Ocean, convergence of the wind was by far the primary component of group velocity convergence. Alternatively, the process can be viewed simply as the growth of a wave or a vortex in convergent background flow. This is represented in a linearized vorticity equation as the product of the background divergence and the disturbance vorticity (e.g., Aiyyer and Molinari 2003).

Holland (1995) argued that the ideas of Webster and Chang (1988) were relevant to the lower-tropospheric flow in the western Pacific. Briegel and Frank (1997) and Ritchie and Holland (1999) noted that tropical cyclone formation events were clustered near the leading edge of the monsoon trough, where westerlies meet easterlies. Sobel and Bretherton (1999) and Kuo et al. (2001) argued that nondivergent barotropic Rossby waves could grow in the same region and provide the seedlings for tropical cyclones. Harr and Elsberry (1991, 1995) showed that tropical cyclogenesis was least likely when no lower-tropospheric westerlies were present in the western Pacific between 5°N and 20°N.

Sobel and Maloney (2000) argued that wave accumulation was strongest during active periods of the MJO. Liebmann et al. (1994) noted that any slowly varying convective background, including the MJO, created a region of slowly varying convergence and cyclonic vorticity that could favor wave growth and subsequent tropical cyclogenesis. Dickinson and Molinari (2002) described a tropical-cyclone-producing mixed Rossby–gravity wave packet that grew within an active MJO and decayed when the MJO passed to the east. Aiyyer and Molinari (2003) showed that in a background flow representative of the MJO, MRG waves in a shallow-
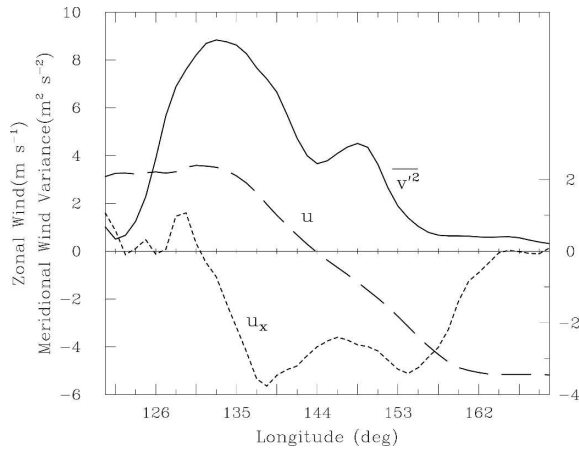
FIG. 6. Background wind at 850 hPa and OLR, each time averaged over the life of the ER wave packet from 14 Aug to 30 Oct 1991. Shading represents OLR $\leq$ 210 W m^{-2}.

water model produced off-equatorial vortices of the scale that could provide seedlings for tropical cyclones. This occurred only when the MJO was asymmetric with respect to the equator.

Taken together, the studies above indicate that wave growth in a convergent background flow makes subsequent tropical cyclogenesis more likely. To examine this process in the current study, Fig. 5 shows the zonal variation of zonal wind, zonal divergence u_x, and wave amplitude. Amplitude was measured by the 15–40-day bandpass-filtered variance of the meridional wind. Each field was averaged from 5°N to 20°N and over the lifetime of the wave packet. Figure 5 shows westerlies to the west and easterlies to the east, creating a u_x magnitude greater than 2.5×10^{-6} s^{-1} between 135° and 155°E. The ER wave amplitude followed the curve of background convergence, with a lag of 5°–10° longitude on the eastern edge. The maximum wave amplitude occurred to the west at nearly the same longitude that convergence returned to zero. Because the waves propagated westward, this is consistent with wave accumulation arguments (e.g., Webster and Chang 1997).

Figure 5 does not show v_y, which had almost the identical shape as u_x with one-third the magnitude, but with opposite sign. As a result, stretching deformation $u_x - v_y$ was more negative than divergence. Regardless, the full convergence substantially exceeded its climatological value in the same region (Sobel and Bretherton 1999). Negative stretching deformation will compress the vorticity contours of the initially long, meridionally constrained waves, but only convergence can increase the magnitude of the vorticity maxima in the waves. As a result, deformation will not be considered further.
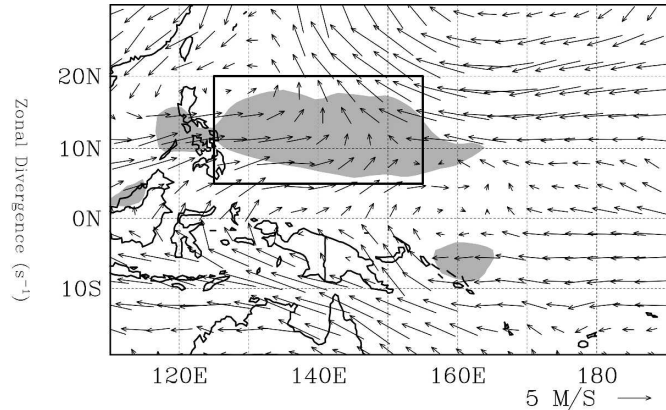
This choice is supported by the results of Kuo et al. (2001), who found that negative stretching deformation without convergence did not produce wave growth.

As noted by Sobel and Bretherton (1999), the wave accumulation concept for westward-propagating waves requires a steady supply of longer waves from the east. Figure 2 provided support for the existence of such waves once the initial gyre formed. Kuo et al. (2001) noted that the wave accumulation reasoning is linear, and nonlinear effects must play an important role in wave growth in the region of vanishing group speed (see also Farrell and Watterston 1985). In addition, once a wave begins to grow, convection is likely to become active and contribute to intensification. By this reasoning, wave accumulation produced the initial intensification of the waves in this study and was the critical factor that allowed subsequent growth by other mechanisms.

Figure 6 shows an x–y plot of background OLR and 850-hPa wind, time averaged as in Fig. 5. The box in this figure indicates the region of the wave packet. The OLR in Fig. 6 is related to the wind in the manner described by Gill (1980), with $u_x < 0$ as westerlies to the west met easterlies to the east at the center of the region of negative OLR anomaly. The Rossby gyre to the northwest of the convective region appears to represent the monsoon trough of the western Pacific. At the equator, weak westerlies far to the west and weak easterlies to the east produced a much smaller background convergence over a larger region. The lack of a focused region of convergence at the equator is consistent with the longer wavelengths of the ER waves at the equator (Fig. 2). The ER wave periods at the equator and at 5°–20°N are identical because wave accumulation does not change the wave period. In the Southern Hemi-

sphere, the only region of convergence occurred at 160°E centered on 5°S, almost exactly where the Southern Hemisphere ER waves appeared in Figs. 3–4. Figures 5 and 6 indicate that the distribution of zonal convergence had an enormous influence on the variation of ER wave properties.

Also likely of significance is the near-zero group speed of the observed packet (Fig. 1b). In the presence of wave accumulation, wave growth occurs when $u_x < 0$ following the group velocity (with respect to the ground). A zero group speed ensures that wave packet growth continues to occur in place. As a result, quasi-stationary forcing, like that shown in Fig. 6, continuously projects onto the wavelength with zero group velocity. Put differently, the forcing projects onto a range of scales, and the dominant scale might be that with a zero group speed, if it exists for the given zonal flow. Table 2 showed that background convergence could eventually reduce the wavelength to one that contained zero group speed for the given zonal flow and that this would occur near the scale of the observed waves.

Overall, the results provide considerable support for wave accumulation as the key mechanism for initial packet growth between 5°N and 20°N. It is notable that this reasoning seems relevant even though the region of $u_x < 0$ is less than one-half the wavelength of the ER waves coming from upstream.

Zhang and Webster (1989) noted that ER waves are much less trapped near the equator in the presence of westerly flow with relatively small latitudinal shear. Figure 6 shows that such background flow existed equatorward of 10°N in the region west of about 150°E. This is the same region in which the ER waves turned poleward. The situation in nature is more complex than that of Zhang and Webster (1989) because the background zonal flow varies in space. Nevertheless, Fig. 6 gives support to the importance of westerly background flow on the behavior of the waves.

Wang and Xie (1996) and Xie and Wang (1996) described an additional large-scale factor that influences the growth of ER waves. They simulated the growth of ER waves with a two-layer model that included parameterizations for wave-scale friction and diabatic heating. In the presence of spatially uniform easterly vertical shear, wave energy was trapped near the surface. Ekman pumping and thus diabatic heating were enhanced, and ER waves grew in amplitude without the presence of background convergence. Maximum growth occurred at wavelengths near 3500 km, remarkably similar to those in this study. When asymmetric vertical shear was imposed, with easterly shear extending well north of the equator but only near the equator
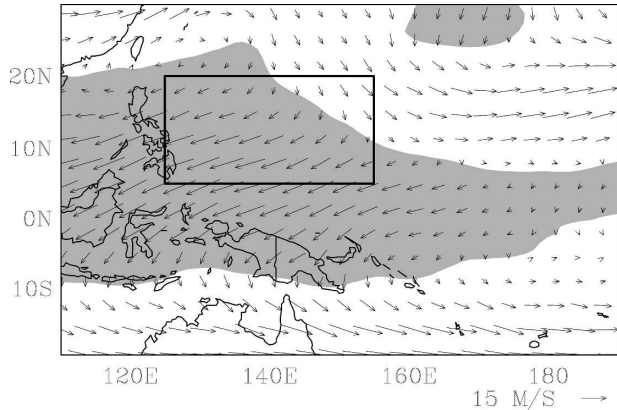

FIG. 7. As in Fig. 6 but for background vertical wind shear vectors between 850 and 200 hPa. Shading indicates the regions in which the vertical wind shear contained an easterly component.

to the south, ER wave growth occurred only in the Northern Hemisphere. In westerly vertical wind shear, lower-tropospheric growth was minimal. Webster and Chang (1997) also noted the importance of easterly wind shear in trapping ER wave energy in the lower troposphere.

Figure 7 shows an x–y plot of 850–200-hPa wind shear vectors averaged over the packet lifetime. Easterly vertical wind shear (indicated by shading) was large within the wave packet region but small or nonexistent to the east. In addition, easterly vertical wind shear existed at packet longitudes down to 10°S, but nowhere poleward of that in the Southern Hemisphere. It is notable that the Southern Hemisphere ER wave low existed only equatorward of 10°S. The observed locations and asymmetries of ER waves were remarkably consistent with the theoretical and numerical arguments presented by Wang and Xie (1996) and Xie and Wang (1996).

The results in this section suggest that the ER wave packet intensified as a result of wave accumulation. Easterly vertical wind shear minimized energy dispersion in the vertical. These mechanisms seem qualitatively sufficient to produce the initial growth of the packet, beyond which nonlinear (Kuo et al. 2001) and diabatic (Xie and Wang 1996) processes could further contribute. The following section deals with the initiation of the wave packet and the possible role of the monsoon gyre.

d. Initiation of the packet

Lander (1994) and Holland (1995) each assigned a key role in the gyre formation to persistent convection associated with an old frontal zone created by the equatorward motion of an upper-tropospheric trough. Un-
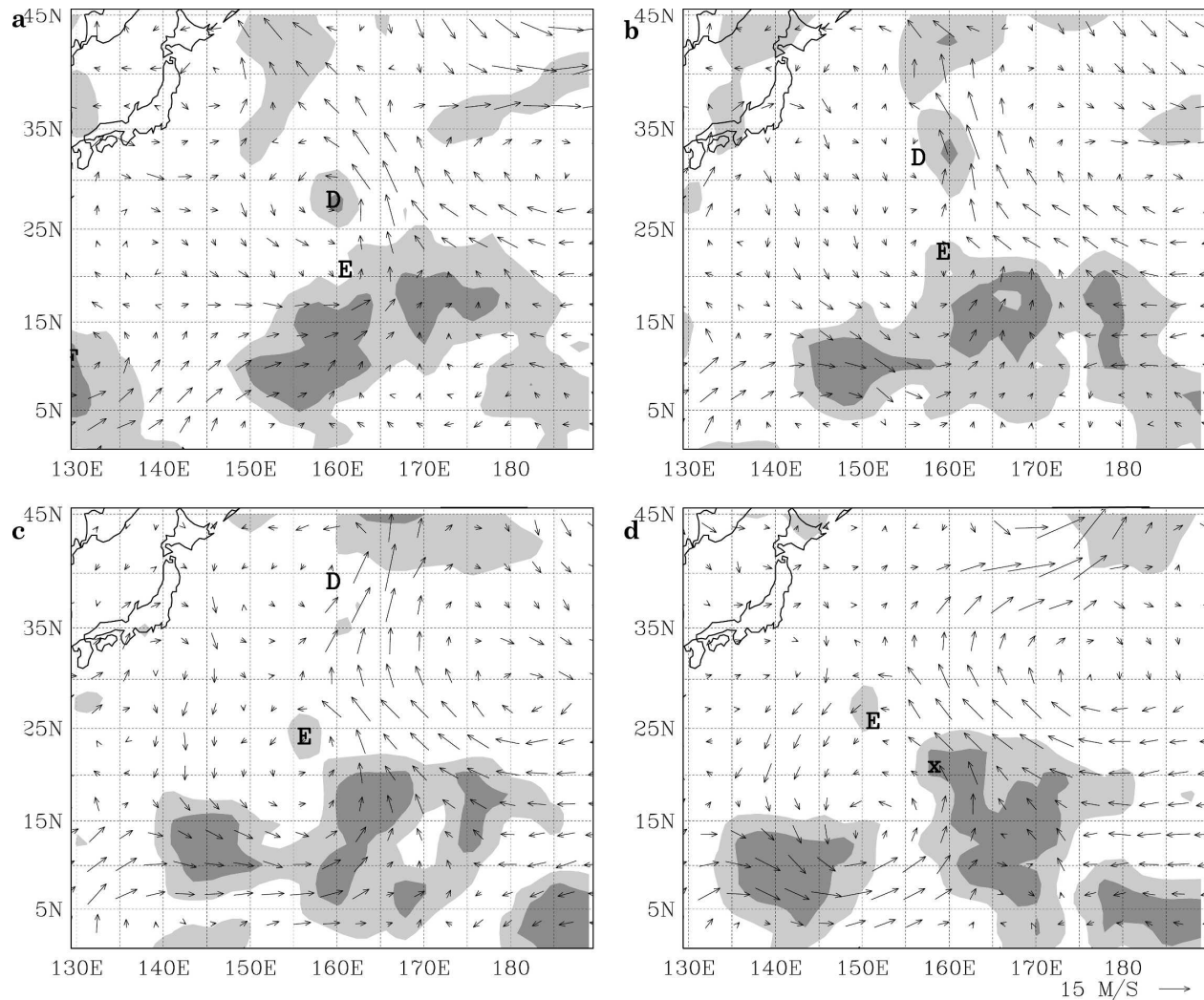
FIG. 8. Unfiltered OLR and 850-hPa wind, once daily at 0000 UTC 9–12 Aug 1991, with OLR shading of 150–210 W m^{-2} (light gray) and <150 W m^{-2} (dark gray). Letters D, E, and x represent the locations of western Pacific tropical cyclones Doug and Ellie and TD 13W, respectively.

filtered daily maps of OLR and 850-hPa vorticity in early August (Lombardo 2004) supported this hypothesis. They indicated a region of strong convection extending from 140° to 170°E that shifted slowly equatorward. A cyclonic gyre developed at 850 hPa near 20°N, northwest of the convective region, on 7 August. On 8 August two disturbances formed in the convection east of this gyre that would become Tropical Cyclones Doug and Ellie. Figure 8 shows daily maps at 0000 UTC of OLR and 850-hPa wind, unfiltered, for the period from 9 to 12 August. On 9 August (Fig. 8a), strong convective heating existed from 5° to 20°N, 150°E to the date line. Tropical Storm Doug had separated from the region of convection. It is difficult to identify a synoptic-scale gyre separate from the tropical cyclone circulations at this time.

By 10 August (Fig. 8b), the two storms moved poleward and the large area of convection continued shifting equatorward. Some indication of a synoptic-scale cyclone was developing near 155°E but it did not contain a closed circulation and may have related in part to flow around future Typhoon Ellie. On 11 August (Fig. 8c), the storms Doug and Ellie completely separated from the convection to the south. A nearly closed synoptic-scale low, which appeared to be associated directly with the convection to its east and south, was better defined near 155°E. Finally, by 12 August (Fig. 8d), a well-defined synoptic-scale low developed near 15°N, 150°E. It is notable that this gyre appeared west of the center of strongest heating, consistent with the modal structure of an ER wave. Figure 8 provides qualitative support for the arguments of Lander (1994)

and Holland (1995) that the gyre formed in a region of persistent active convection.

Off-equatorial asymmetric heating projects efficiently onto ER waves (Zhang and Webster 1992; Hoskins and Yang 2000; Sobel and Horinouchi 2000). Although the gyre was an isolated low that did not contain ER wave structure when it formed, such structure developed within a single wave period. Similar behavior occurred in the simulations of Sobel and Horinouchi (2000). It is argued that the heating associated with the convection in Fig. 8 excited the initial ER wave low. The stationary ER wave packet subsequently intensified in the persistent convergent background flow associated with the monsoon trough (Fig. 6). The monsoon gyre is seen as simply the initial low in the packet. As the gyre formed, tropical depression 13W ("x" in Fig. 8d) developed to its east on 11 August. The storm destined to be Typhoon Gladys formed east of the gyre on 13 August. The process of repeated tropical cyclogenesis is investigated in the following section.

e. Tropical cyclogenesis

Of the 13 western Pacific storms during the lifetime of the wave packet, 11 formed east of a 15–40-day bandpass-filtered low. To determine whether the formation of each storm could be associated with the ER wave packet, four criteria were employed: (i) the 15–40-day ER wave low occurred within the wave packet; (ii) the storm formed within a bandpass-filtered cyclonic vorticity anomaly that extended eastward from a stronger vorticity maximum at the center of the ER wave low; (iii) the storm developed within or no more than 100 km from a negative bandpass-filtered OLR anomaly of at least 10 W m^{-2} that extended from east or south of the primary ER wave low; and (iv) the storm formed within one-half wavelength (about 1800 km) east of the ER wave low. Table 3 shows the results of this analysis. Eight of the 13 storms met all of the criteria. The formations of these eight were labeled as "ER wave related." One other storm met all but the fourth criterion and was listed as uncertain. This storm was not included in any composites. The formations of the remaining four storms were judged to be unrelated to ER wave activity.

The environment at the time of tropical cyclone formation will be shown using two composites of OLR and 850-hPa winds and vorticity: (i) a bandpass-filtered composite with respect to the 850-hPa vorticity maximum of the ER wave primary low and (ii) an unfiltered composite with respect to the location of tropical cyclone formation. Because tropical cyclones formed at both ends of the wave packet, the ER-wave-related

TABLE 3. List of western Pacific tropical cyclones during the lifetime of the ER wave packet. All storms are included that formed on or after 11 August 1991, as the monsoon gyre was developing, up to the end of the packet, taken as 30 October 1991. Each storm is labeled as to whether or not its formation was associated with the packet, following the four criteria given in the text. Those storms associated with ER waves are identified as "eastern" (forming east of 135°E; six total) or "western" (forming at the western end of the packet; two total). The storm listed as "uncertain" is not included in the composites in Figs. 9a, 10, and 11. The mean formation location of the eastern subset was 15.3°N, 151.6°E and for the western subset it was 19.2°N, 129.3°E.

Storm name	Formation date	ER wave related? (see text)	Formation type
TD 13W	11 Aug	Yes	Eastern
Gladys	13 Aug	Yes	Eastern
TD 15W	21 Aug	Yes	Eastern
Harry	27 Aug	Yes	Western
Ivy	31 Aug	No	—
Joel	01 Sep	Yes	Western
Kinna	08 Sep	Yes	Eastern
Luke	13 Sep	No	—
Mirielle	13 Sep	No	—
Nat	15 Sep	No	—
Orchid	01 Oct	Yes	Eastern
Pat	01 Oct	Uncertain	Eastern
Ruth	16 Oct	Yes	Eastern

storms were divided into two groups for compositing. Six storms developed east of 135°E. These six storms make up the "eastern composite." The two storms that formed near the western edge of the packet make up the "western composite." This two-storm composite does not contain much statistical significance, but will be shown because it displays the dramatic change in structure of the ER wave lows as they passed through the convergent background. The mean location of formation for the eastern composite was 15.3°N, 151.6°E; for the western composite 19.2°N, 129.3°E.

Figures 9a,b show the locations of tropical cyclone formation with respect to the bandpass-filtered vorticity maximum within the primary ER wave low for the eastern and western composites, respectively. Figure 9a has its southern boundary near 5°S. It shows the structure apparent from Figs. 3 and 4 with an ER wave high to the northwest of the low. Cyclonic vorticity extended farther east of the low than west, and convection was strongest about 1200 km east-southeast of the low center. As noted earlier, this composite ER wave structure closely resembles that found by Wheeler et al. (2000). Every tropical cyclone in this composite formed east of the bandpass-filtered ER wave low in the convectively active region.

Figure 9b shows the location of storm formation for the western composite. The southern boundary of this
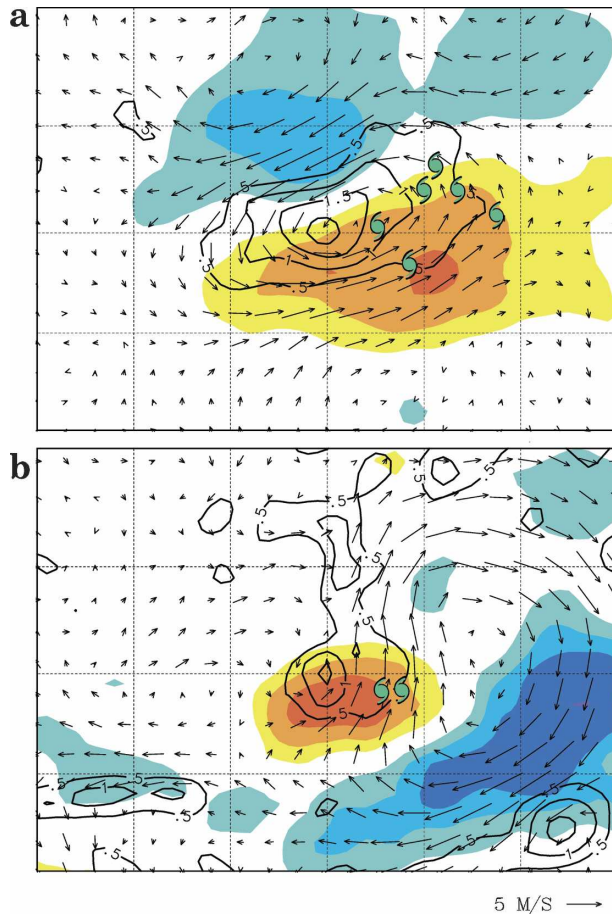
FIG. 9. Bandpass-filtered (15–40 day) OLR and 850-hPa winds and vorticity, composited about the 15–40-day ER wave vorticity maximum. Hurricane symbols indicate the location of storm formation with respect to the ER wave vorticity maximum. OLR shading represents ± 10, 20, and 30 W m^{-2}. Only cyclonic vorticity is contoured, starting at 0.5×10^{-5} s^{-1} in increments of 0.5×10^{-5} s^{-1}. (a) Eastern composite of the six storms that formed east of 135°E; (b) western composite of the two storms that formed west of 135°E, near the western end of the wave packet. Latitude and longitude lines are plotted in 10° increments.
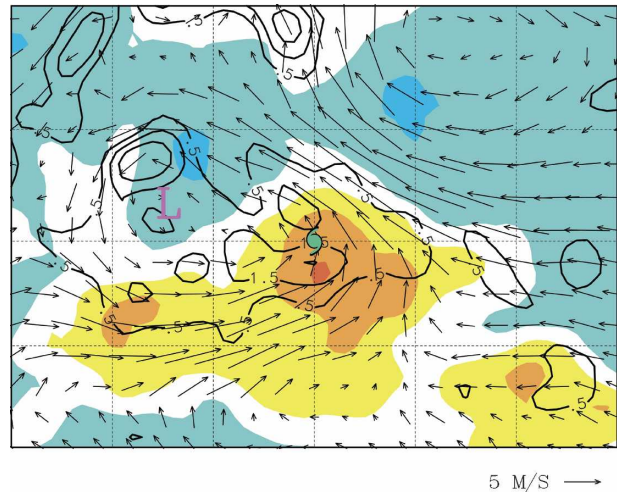

FIG. 10. Unfiltered OLR and unfiltered 850-hPa wind and vorticity, composited with respect to the genesis location of six ER-wave-related tropical cyclones that formed east of 135°E. The mean genesis location, indicated by the hurricane symbol, lies at 15.3°N, 151.6°E. The magenta "L" indicates the circulation center of the ER wave low in the unfiltered field. OLR shading is as follows: (red) ≤ 150 W m^{-2}; (orange) 150–180 W m^{-2}; (yellow) 180–210 W m^{-2}; (light blue) 240–270 W m^{-2}; (darker blue) >270 W m^{-2}. Only three vorticity contours are shown: 0.5, 1.5 and 2.5 $\times 10^{-5}$ s^{-1}. Latitude and longitude lines are plotted in 10° increments.

composite lies at about 1°S. Once again convection and cyclonic vorticity extended eastward from the center of the ER wave low, and the storms formed to the east. In this composite, however, the lows were much smaller scale after passing through the convergent background. The anticyclonic anomaly to the east and southeast fell within the middle of the wave packet at the times of this composite and was much stronger and larger than the low.

Figure 10 shows a composite of unfiltered fields about the formation point of each storm in the eastern composite. Figure 10 confirms that active convection, a secondary cyclonic vorticity maximum, and tropical cy-

clone formation occurred east of the center of circulation of the composite ER wave low.

Frank and Roundy (2006) showed that cyclogenesis in the western Pacific occurred a few hundred kilometers southeast of a composite ER wave low, consistent with Figs. 9 and 10. In addition, Bessafi and Wheeler (2006) showed that storms generally formed in regions of active convection and cyclonic vorticity. In contrast to this study, Bessafi and Wheeler (2006) found that tropical cyclogenesis occurred about equally east and west of the ER wave lows in the south Indian Ocean. Their results might reflect regional differences in ER wave structure, or possibly the different filtering used to identify the ER waves (see the discussion in section 2).

Figure 11 shows unfiltered 850–200-hPa vertical wind shear vectors and their magnitude, again composited about the genesis points of the eastern formation composite. The shaded regions indicate wind shear exceeding 10 m s^{-1}. Storm formation did not occur in the active convection to the south of the ER wave low, where vertical wind shear was large. Formation also did not occur in the region of minimum vertical wind shear northeast of the low, which was convectively inactive. Rather, the storms developed in a region of moderate vertical shear that contained both strong convection and cyclonic vorticity.
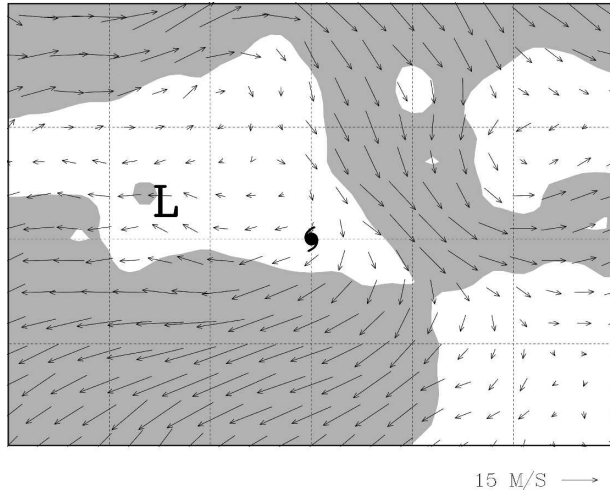
FIG. 11. As in Fig. 10 but for unfiltered 850–200-hPa vertical wind shear vectors. Shading represents regions in which the vertical wind shear magnitude exceeded 10 m s^{-1}. The "L" represents the circulation center of the ER wave low in Fig. 10.

4. Discussion

a. Equatorial Rossby wave packet

A lower-tropospheric wave packet was described in this study that lasted 2.5 months. Waves within the packet obeyed the dispersion relation for equatorial Rossby waves for an equivalent depth near 25 m when the influence of nonzero background zonal flow was included. The waves had a period of 22 days, a wavelength of 3600 km, a westward phase speed of 1.9 m s^{-1}, and a near-zero group speed. Two questions about the packet were raised earlier (section 3b): why the packet became so strong and long lasting and why wave properties differed so much with latitude. The evidence presented in this paper suggests that two properties of the background flow created this behavior: lower-tropospheric zonal wind convergence and easterly vertical wind shear. In the manner described by Webster and Chang (1988), Chang and Webster (1990), and Holland (1995), strongly convergent flow between 5° and 20°N produced both an amplification and a zonal-scale contraction of waves reaching the region from the central Pacific. This background convergence was collocated with a region of persistent convective heating associated with the monsoon trough in the western Pacific. Maximum wave amplitude occurred at the western end of the convergent region, consistent with the wave accumulation hypothesis. The wave accumulation argument appears valid even though the convergent region width of about 3500 km was less than half of the initial upstream wave scale. At the equator, convergence was weak and occurred on a much larger scale,

producing little scale contraction of the waves. In the Southern Hemisphere, background convergence was restricted to one small region, and only in that region did ER waves show significant amplitude.

The wave accumulation reasoning in the previous paragraph is consistent with the ideas of Ritchie and Holland (1999), Sobel and Bretherton (1999), and Kuo et al. (2001). In this case the relevant waves were equatorial Rossby waves rather than nondivergent barotropic Rossby waves, whose phase and group speeds differ dramatically.

The background flow was also characterized by large easterly vertical wind shear, both locally near the level of largest wave amplitude at 850 hPa (not shown) and over the 850–200-hPa layer (Fig. 11). This favored both trapping of wave energy at low levels and enhanced wave growth by frictional and diabatic effects (Wang and Xie 1996; Xie and Wang 1996). In the current study, wave growth did not occur in the absence of either low-level convergence or easterly vertical wind shear in the background flow. Both factors likely played a role in the large observed wave amplitude.

Lander (1994) and Holland (1995) attributed the growth of the monsoon gyre to a localized region of strong heating in early August associated with equatorward penetration of an upper-tropospheric trough. Kiladis and Wheeler (1995) argued that the same mechanism will excite an equatorial Rossby wave. Consistent with both of these papers, it is argued here that the gyre represented the initial ER wave low pressure area. The convergent background flow insured that a wave packet would develop and amplify. A series of ER waves from the east grew within the packet during the following two months.

b. Tropical cyclogenesis within ER waves

During the lifetime of the wave packet 13 storms developed in the western Pacific. A storm was labeled ER wave related if it developed within one-half wavelength to the east of a bandpass-filtered ER wave low within the packet and if development occurred within an extended region of bandpass-filtered cyclonic vorticity and active convection. Using these criteria, 8 of 13 storms were associated with the ER wave packet. These results are consistent with the composite ER wave results of Frank and Roundy (2006), who showed that genesis occurred several hundred kilometers southeast of the ER wave low center.

Based on the composite structure, the following sequence of events is hypothesized to produce tropical cyclones within the ER wave packet: relatively small-amplitude, long ER waves propagated westward, grew in amplitude, and contracted in scale within the conver-

gent background and stationary wave packet. Convection intensified east of the ER wave lows, consistent with their theoretical structure, as the waves amplified. This produced smaller-scale vorticity maxima east of the ER wave low that provided the seedlings for tropical cyclones. The long period and slow motion of waves within the packet maximized the opportunity for tropical cyclones to form. Figure 11 shows that storms formed in a region of moderate vertical shear. The fact that storms did not form where vertical wind shear was smallest suggests that the positive impacts of wave-induced convection and cyclonic vorticity were of greater importance than those of wave-induced vertical wind shear. This supports the findings of Bessafi and Wheeler (2006) in the south Indian Ocean.

The results of this paper, along with the studies of Yamazaki and Murakami (1989), Hartmann et al. (1992), Numaguti (1995), Bessafi and Wheeler (2006), and Frank and Roundy (2006), suggest that ER waves might have a substantial influence on tropical cyclogenesis. The western Pacific contains a climatological region of lower-tropospheric convergence (e.g., Holland 1995; Sobel and Bretherton 1999) and easterly wind shear at the same latitudes where ER wave lows are found. This allows the mechanisms of Webster and Chang (1988) and Xie and Wang (1996) to produce amplification and scale contraction of ER waves. Frank and Roundy (2006) found that ER waves contained their largest variance in the northwest Pacific during boreal summer. Hartmann et al. (1992) found that 20–25-day waves in the west Pacific (likely ER waves) had large amplitude in late boreal summer and fall. The above results suggest that ER waves might represent a common precursor disturbance for tropical cyclones in the northwest Pacific Ocean during the peak of the season.

REFERENCES

Aiyyer, A. R., and J. Molinari, 2003: Evolution of mixed Rossby–gravity waves in idealized MJO environments. *J. Atmos. Sci.,* **60,** 2837–2855.

Bessafi, M., and M. C. Wheeler, 2006: Modulation of south Indian Ocean tropical cyclones by the Madden–Julian oscillation and convectively coupled equatorial waves. *Mon. Wea. Rev.,* **134,** 638–656.

Briegel, L. M., and W. M. Frank, 1997: Large-scale influences on tropical cyclogenesis in the western North Pacific. *Mon. Wea. Rev.,* **125,** 1397–1413.

Chang, C.-P., J. M. Chen, P. A. Harr, and L. E. Carr, 1996: Northwestward-propagating wave patterns over the tropical western North Pacific during summer. *Mon. Wea. Rev.,* **124,** 2245–2266.

Chang, H.-R., and P. J. Webster, 1990: Energy accumulation and emanation at low latitudes. Part II: Nonlinear response to strong episodic equatorial forcing. *J. Atmos. Sci.,* **47,** 2624–2644.

Dickinson, M., and J. Molinari, 2002: Mixed Rossby–gravity waves and western Pacific tropical cyclogenesis. Part I: Synoptic evolution. *J. Atmos. Sci.,* **59,** 2183–2196.

Farrell, B., and I. Watterson, 1985: Rossby waves in opposing currents. *J. Atmos. Sci.,* **42,** 1746–1756.

Frank, W. M., and P. E. Roundy, 2006: The role of tropical waves in tropical cyclogenesis. *Mon. Wea. Rev.,* **134,** 2397–2417.

Gill, A. E., 1980: Some simple solutions for heat-induced circulation of the tropical atmospheres. *Quart. J. Roy. Meteor. Soc.,* **106,** 447–462.

Harr, P. A., and R. L. Elsberry, 1991: Tropical cyclone track characteristics as a function of large-scale circulation anomalies. *Mon. Wea. Rev.,* **119,** 1448–1468.

——, and ——, 1995: Large-scale circulation variability over the tropical western North Pacific. Part I: Spatial patterns and tropical cyclone characteristics. *Mon. Wea. Rev.,* **123,** 1225–1246.

Hartmann, D. L., M. L. Michelsen, and S. A. Klein, 1992: Seasonal variations of tropical intraseasonal oscillations: A 20–25-day oscillation in the western Pacific. *J. Atmos. Sci.,* **49,** 1277–1289.

Holland, G. J., 1995: Scale interaction in the western Pacific monsoon. *Meteor. Atmos. Phys.,* **56,** 57–79.

Hoskins, B. J., and G.-Y. Yang, 2000: The equatorial response to higher-latitude forcing. *J. Atmos. Sci.,* **57,** 1197–1213.

Kiladis, G. N., and M. Wheeler, 1995: Horizontal and vertical structure of observed tropospheric equatorial Rossby waves. *J. Geophys. Res.,* **100,** 22 981–22 998.

Kuo, H.-C., J.-H. Chen, R. T. Williams, and C.-P. Chang, 2001: Rossby waves in zonally opposing mean flow: Behavior in northwest Pacific summer monsoon. *J. Atmos. Sci.,* **58,** 1035–1050.

Lanczos, C., 1956: *Applied Analysis.* Prentice-Hall, 539 pp.

Lander, M. A., 1994: Description of a monsoon gyre and its effects on the tropical cyclones in the western North Pacific during August 1991. *Wea. Forecasting,* **9,** 640–654.

Liebmann, B., and C. Smith, 1996: Description of a complete (interpolated) outgoing longwave radiation dataset. *Bull. Amer. Meteor. Soc.,* **77,** 1275–1276.

——, H. H. Hendon, and J. D. Glick, 1994: The relationship between tropical cyclones of the western Pacific and Indian Oceans and the Madden–Julian oscillation. *J. Meteor. Soc. Japan,* **72,** 401–411.

Lighthill, J., 1978: *Waves in Fluids.* Cambridge University Press, 504 pp.

Lindzen, R. D., 1967: Planetary waves on beta-planes. *Mon. Wea. Rev.,* **95,** 441–451.

Lombardo, K., 2004: Influence of equatorial Rossby waves on tropical cyclogenesis in the western Pacific. M.S. thesis, Dept.

of Earth and Atmospheric Sciences, University at Albany, State University of New York, 135 pp.

Matsuno, T., 1966: Quasi-geostrophic motions in the equatorial area. *J. Meteor. Soc. Japan,* **44,** 25–43.

Nitta, T., and Y. Takayabu, 1985: Global analysis of the lower tropospheric disturbances in the Tropics during the northern summer of the FGGE year. Part II: Regional characteristics of the disturbances. *Pure Appl. Geophys.,* **123,** 272–292.

Numaguti, A., 1995: Characteristics of 4-to-20-day-period disturbances observed in the equatorial Pacific during the TOGA COARE IOP. *J. Meteor. Soc. Japan,* **73,** 353–377.

Ritchie, E. A., and G. J. Holland, 1999: Large-scale patterns associated with tropical cyclogenesis in the western Pacific. *Mon. Wea. Rev.,* **127,** 2027–2043.

Roundy, P. E., and W. M. Frank, 2004: A climatology of waves in the equatorial region. *J. Atmos. Sci.,* **61,** 2105–2132.

Sobel, A. H., and C. S. Bretherton, 1999: Development of synoptic-scale disturbances over the summertime tropical northwest Pacific. *J. Atmos. Sci.,* **56,** 3106–3127.

——, and T. Horinouchi, 2000: On the dynamics of easterly waves, monsoon depressions, and tropical depression type disturbances. *J. Meteor. Soc. Japan,* **78,** 167–173.

——, and E. D. Maloney, 2000: Effect of ENSO and the MJO on western North Pacific tropical cyclones. *Geophys. Res. Lett.,* **27,** 1739–1742.

Straub, K. H., and G. N. Kiladis, 2002: Observations of a convectively coupled Kelvin wave in the eastern Pacific ITCZ. *J. Atmos. Sci.,* **59,** 30–53.

Takayabu, Y. N., 1994: Large-scale cloud disturbances associated with equatorial waves. I: Spectral features of the cloud disturbances. *J. Meteor. Soc. Japan,* **72,** 433–448.

——, and T. Nitta, 1993: 3–5 day-period disturbances coupled with convection over the tropical Pacific Ocean. *J. Meteor. Soc. Japan,* **71,** 221–245.

Wallace, J. M., and V. E. Kousky, 1968: Observational evidence of Kelvin waves in the tropical stratosphere. *J. Atmos. Sci.,* **25,** 900–907.

Wang, B., and X. Xie, 1996: Low-frequency equatorial waves in vertically sheared zonal flow. Part I: Stable waves. *J. Atmos. Sci.,* **53,** 449–467.

Webster, P. J., and H.-R. Chang, 1988: Equatorial energy accumulation and emanation regions: Impacts of a zonally varying basic state. *J. Atmos. Sci.,* **45,** 803–829.

——, and ——, 1997: Atmospheric wave propagation in heterogeneous flow: Basic flow constraints on tropical–extratropical interaction and equatorial wave modification. *Dyn. Atmos. Oceans,* **27,** 91–134.

Wheeler, M., and G. N. Kiladis, 1999: Convectively coupled equatorial waves: Analysis of clouds and temperature in the wavenumber–frequency domain. *J. Atmos. Sci.,* **56,** 374–399.

——, ——, and P. J. Webster, 2000: Large-scale dynamical fields associated with convectively coupled equatorial waves. *J. Atmos. Sci.,* **57,** 613–640.

Xie, X., and B. Wang, 1996: Low-frequency equatorial waves in vertically sheared zonal flow. Part II: Unstable waves. *J. Atmos. Sci.,* **53,** 3589–3605.

Yamazaki, N., and M. Murakami, 1989: An intraseasonal amplitude modulation of the short-term tropical disturbances over the western Pacific. *J. Meteor. Soc. Japan,* **67,** 791–807.

Yanai, M., and T. Maruyama, 1966: Stratospheric wave disturbances propagating over the equatorial Pacific. *J. Meteor. Soc. Japan,* **44,** 291–294.

Zhang, C., and P. J. Webster, 1989: Effects of zonal flows on equatorially trapped waves. *J. Atmos. Sci.,* **46,** 3632–3652.

——, and ——, 1992: Laterally forced equatorial perturbations in a linear model. Part I: Stationary transient forcing. *J. Atmos. Sci.,* **49,** 585–607.